FIGURE S1

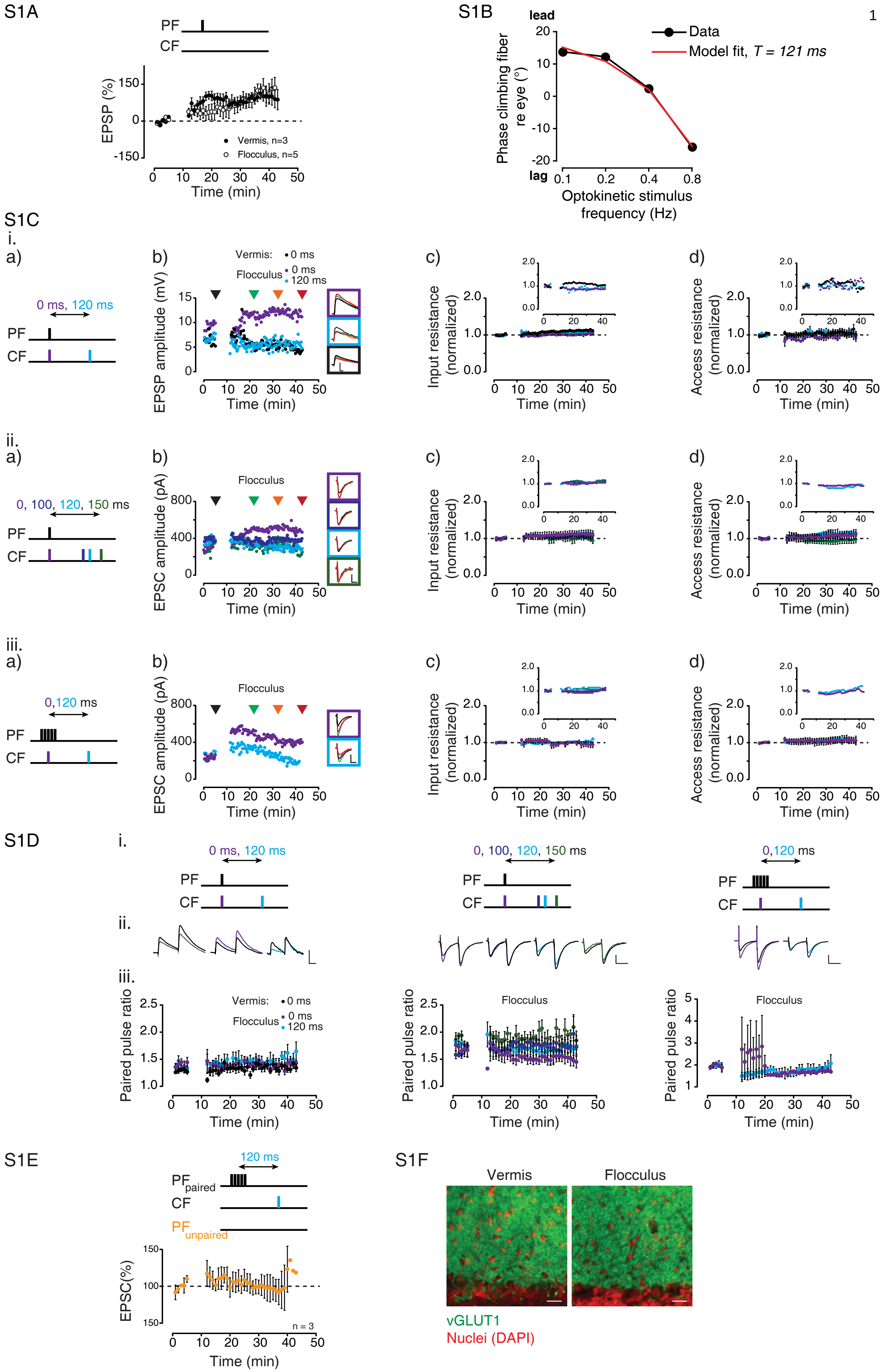
S1A
PF
CF
EPSP (%)
150
0
-150
Vermis, n=3
Flocculus, n=5
Time (min)
S1B
lead
lag
Data
Model fit, T = 121 ms
Phase climbing fiber re eye (°)
Optokinetic stimulus frequency (Hz)
S1C
i.
a)
0 ms, 120 ms
PF
CF
b)
Vermis: 0 ms
Flocculus 0 ms 120 ms
EPSP amplitude (mV)
Time (min)
c)
Input resistance (normalized)
d)
Access resistance (normalized)
ii.
0, 100, 120, 150 ms
Flocculus
EPSC amplitude (pA)
iii.
0,120 ms
S1D
i.
ii.
iii.
0 ms, 120 ms
0, 100, 120, 150 ms
0,120 ms
Paired pulse ratio
Vermis: 0 ms
Flocculus 0 ms 120 ms
Flocculus
Time (min)
S1E
120 ms
PFpaired
CF
PFunpaired
EPSC(%)
n = 3
Time (min)
S1F
Vermis
Flocculus
vGLUT1
Nuclei (DAPI)

Supplemental Figure Legends

Supplemental Figure 1 (related to Figure 1)

Fig. S1A. Parallel fiber stimulation alone induced LTP in both the vermis and the flocculus. Non-associative plasticity was induced by PF stimulation alone (300 times at 1Hz, *top schematic),* in both the vermis and the flocculus. n = number of cells, mean ± S.E.M.

Fig. S1B. Estimated climbing fiber delays in flocculus of mouse.
The delay between retinal image motion, which signals an oculomotor performance error, and climbing fiber responses in the mouse flocculus was estimated using the same analysis used previously in nonhuman primates (Raymond and Lisberger, 1998). Climbing fiber firing was inferred from the complex spikes recorded from Purkinje cells during optokinetic reflex adaptation (Goossens et al., 2004). The phase of the climbing fiber response relative to the visual stimulus (θ) was fit with a fixed delay:

$$\theta = R + 2\pi f T$$

where *T* is the climbing fiber delay, *f* is the frequency of the stimulus and *R* is a constant reference point on the visual stimulus. The best fit to the data was obtained with a value of 121 ms for the delay, *T*, and a value of 19.6° for *R*. The estimated delay in mice is very similar to the 122 ms delay estimated in nonhuman primates, which supported the prediction that it would be optimal for climbing fiber activity to induce plasticity at synapses active ~122 ms earlier (Raymond & Lisberger, 1998). (See Supplemental Procedures for more details.)

Fig. S1C. Long-term depression of parallel fiber-to-Purkinje cell synapses is induced by a PF-CF pairing interval of 120 ms and not 0 ms: example cells, and measurements of input and access resistance.

i) Long-term plasticity measured in current clamp (related to Fig. 1A, B). a) Schematic showing PF-CF interval, corresponding colors are used in *b-d*. **b)** Example cells for each condition tested. *Inset, right:* Traces showing individual EPSPs for each example cell, boxed in corresponding color. Traces were measured at times indicated by the *colored arrowheads - Black*: at min. 4-5 before the induction of plasticity; *green*: at min. 8-10 after induction of plasticity; *orange*: min. 18-20; *red*: min. 28-30. Scale bars: 5 mV, 20 ms. **c)** Input resistance, normalized to baseline, for all cells used for analysis of LTD measured in current clamp in Fig. 1A, B. *Inset:* input resistance for example cells shown in *b*. **d)** Access resistance, normalized to baseline, for all cells used for analysis of LTD measured in current clamp in Fig. 1A, B. *Inset:* access resistance for example cells shown in *b*.

ii) Long-term plasticity measured in voltage clamp (related to Fig. 1C). a) Schematic showing PF-CF interval, corresponding colors are used in *b-d*. **b)** Example cells for each PF-CF pairing interval. *Inset, right:* traces showing individual EPSCs for each example cell, boxed in corresponding color, measured at times indicated by the colored arrowheads as in Fig. S1Cib. Scale bars: 200 pA, 20 ms. **c)** Input resistance for all cells shown in Fig. 1C. *Inset:* input resistance for example cells shown in *b*. **d)** Access resistance for all cells shown in in Fig. 1C. *Inset:* access resistance for example cells shown in *b*.

iii) Long-term plasticity induced by pairing a train of PF stimuli with the CF stimulus (related to Fig. 1D). a) Schematic showing PF-CF interval, corresponding colors are used in *b-d*. **b)** Example cells for each PF-CF pairing interval. *Inset, right:* traces showing individual EPSCs for each example cell, boxed in corresponding color, measured at times indicated by the colored arrowheads. Scale bars: 200 pA, 20 ms. **c)** Input resistance for all cells shown in Fig. 1D. *Inset:* input resistance for example cells shown in *b*. **d)** Access resistance for all cells shown in Fig. 1D. *Inset:* access resistance for example cells shown in *b*. All panels: mean ± S.E.M.

Fig. S1D. Long-term depression is not accompanied by a change in paired pulse ratio. i) Schematics showing PF-CF interval for each column in Fig. S1D, with different PF-CF intervals identified by color, and corresponding colors used in *ii-iii*. **ii)** Example traces for average data shown below in *iii*, where black = min 5, before plasticity induction, and corresponding color = 30 min after induction. Scale bars: *left:* 5 mV, 50 ms, *middle, right:* 200 pA, 40 ms. **iii)** Average paired pulse ratio for experiments on long-term plasticity. *Left:* Current clamp experiments in the flocculus and the vermis, shown in Fig 1A,B. *Middle:* Voltage clamp experiments in the flocculus, with plasticity induced by single parallel fiber stimuli paired with climbing fiber stimuli, shown in Fig 1C. *Right:* Voltage clamp experiments in the flocculus, with plasticity induced by pairing trains of parallel fiber stimuli with climbing fiber stimuli, shown in Fig 1D. Mean ± S.E.M. LTD in the flocculus, induced using both single parallel fiber stimuli and trains, appeared to be expressed post-synaptically, as previously described for cerebellar LTD (Chung et al., 2003; Linden, 2012), since there was no change in the paired-pulse ratio.

Fig. S1E. Long-term depression was not expressed in an unpaired control pathway. For long-term plasticity experiments shown in Fig. 1D, two parallel fiber pathways were stimulated for some cells recorded in the flocculus. One pathway was paired with climbing fiber stimulation (PF_{paired}), while the other pathway was not paired with CF stimulation ($PF_{unpaired}$). The amplitude of the EPSC elicited by stimulation of each PF pathway was tested in an interleaved fashion, before and after pairing of PF_{paired} with CF stimulation (300 times at 1 Hz). No LTD was induced in the $PF_{unpaired}$ pathway. n = number of cells, mean ± S.E.M.

Fig. S1F. Similar staining of parallel fiber synapses, marked by VGLUT1, in slices of vermis and flocculus. Parallel fiber synapses were stained with an antibody against VGLUT1 (green), and nuclei were stained with DAPI (red), both pseudocolored, in sagittal slices of the cerebellar vermis and coronal slices of the cerebellar flocculus. Scale bar is 20 µm.

FIGURE S2

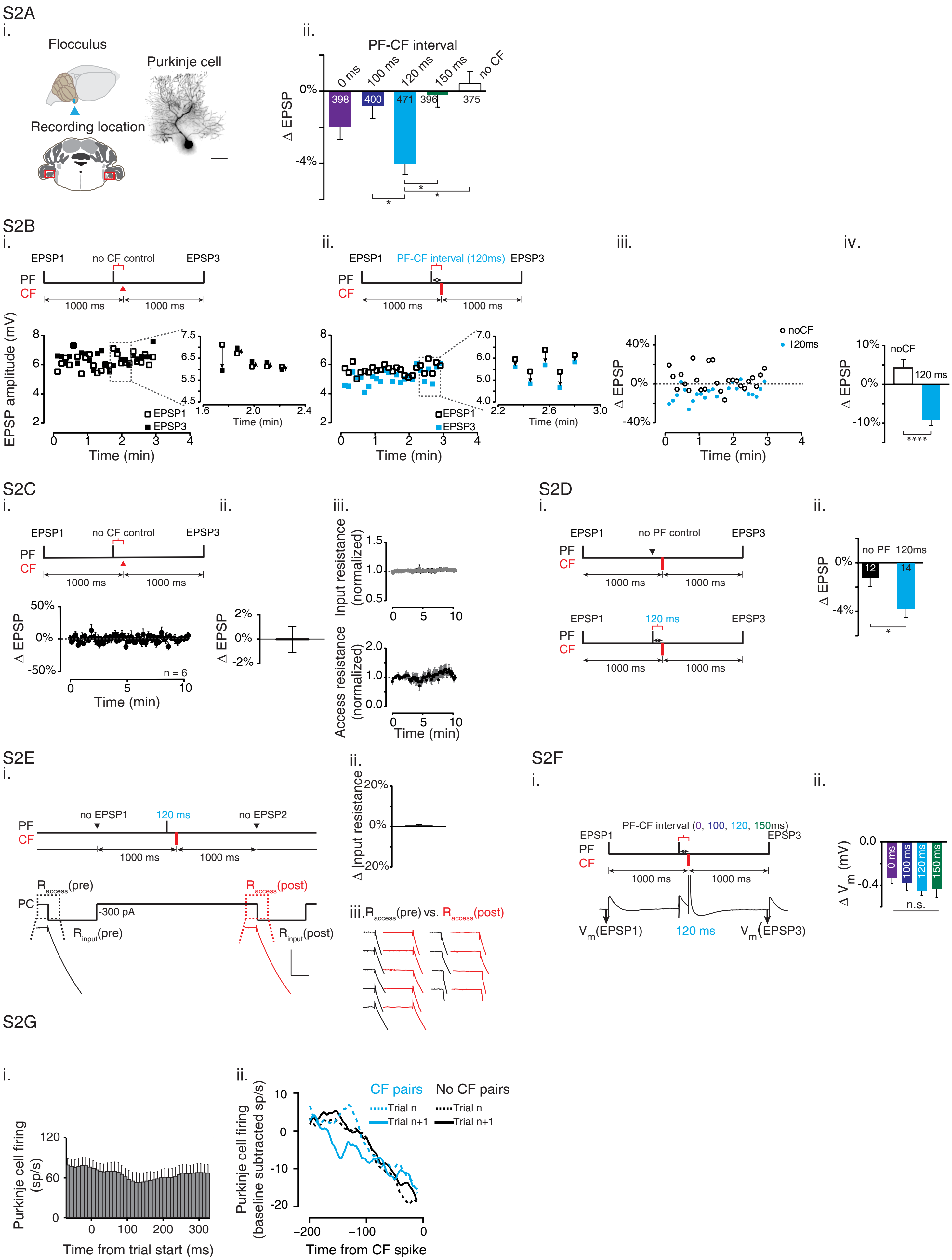
S2A
i.
Flocculus
Purkinje cell
Recording location
ii.
PF-CF interval
0 ms
100 ms
120 ms
150 ms
no CF
0%
-4%
Δ EPSP
398
400
471
396
375
S2B
i.
EPSP1
no CF control
EPSP3
PF
CF
1000 ms
1000 ms
EPSP amplitude (mV)
Time (min)
Time (min)
EPSP1
EPSP3
ii.
PF-CF interval (120ms)
iii.
noCF
120ms
40%
0%
-40%
Δ EPSP
iv.
10%
0%
-10%
noCF
120 ms
****
S2C
i.
EPSP1
no CF control
EPSP3
50%
0%
-50%
Δ EPSP
n = 6
Time (min)
ii.
2%
0%
-2%
iii.
Input resistance (normalized)
Access resistance (normalized)
Time (min)
S2D
i.
EPSP1
no PF control
EPSP3
120 ms
ii.
no PF
120ms
12
14
0%
-4%
S2E
i.
no EPSP1
120 ms
no EPSP2
PC
R access (pre)
-300 pA
R input (pre)
R access (post)
R input (post)
ii.
20%
0%
-20%
Δ Input resistance
iii. R access (pre) vs. R access (post)
S2F
i.
PF-CF interval (0, 100, 120, 150ms)
EPSP1
EPSP3
Vm(EPSP1)
120 ms
Vm(EPSP3)
ii.
0.0
-0.4
Δ Vm (mV)
0 ms
100 ms
120 ms
150 ms
n.s.
S2G
i.
Purkinje cell firing (sp/s)
Time from trial start (ms)
ii.
CF pairs
No CF pairs
Trial n
Trial n+1
Trial n
Trial n+1
Purkinje cell firing (baseline subtracted sp/s)
Time from CF spike

Supplemental Figure 2 (related to Figure 2)

Fig. S2A. Single-trial plasticity in the flocculus, analyzed by averaging across trials rather than across cells shows the most depression at a PF-CF interval of 120 ms. i) *Top left:* Flocculus shown in blue (*arrowhead*). *Bottom left:* Recording location in a coronal plane (*red boxes*). *Right:* Dye-filled Purkinje cell from the flocculus, scale bar 20 µm. Maximum-intensity projection of Z-stacks. Gamma-filtering was used on each image of a Z-stack to compensate for differences in absolute intensity along the depth of the slice (see Supplemental Procedures). **ii)** Single-trial data from the flocculus, shown in Fig. 2B, analyzed by pooling the 19-25 trials at each PF-CF interval for each cell, across all cells and then averaging, instead of using a single average value for each PF-CF interval for each cell. * $p < 0.05$, one way ANOVA on ranks followed by Dunn's pairwise comparison, n = number of trials, mean ± S.E.M.

Fig. S2B. Single trial plasticity in the flocculus: example cell. i, ii) Measurement of single-trial plasticity is illustrated in one example cell in the flocculus. *Top schematics* illustrate experimental design, where PF stimulation was either presented alone (*i, no CF; red arrowhead* indicates omitted CF stimulus*)*, or paired with CF stimulation (*ii, 120 ms PF-CF interval).* The amplitudes of EPSP1 (*open black squares*) and EPSP3 (*filled black, filled blue*) from each of 25 consecutive trials are plotted, to show the fluctuations in EPSP amplitude. *(i)* For the no CF control, there was no consistent difference between EPSP1 and EPSP3. *Inset:* Expanded section showing both increases and decreases from EPSP1 to EPSP3 on individual trials. *(ii)* For a PF-CF pairing interval of 120 ms, the EPSP was consistently smaller post-pairing (EPSP3, *blue*), as compared with pre-pairing (EPSP1, *open squares*), illustrated in the expanded inset section. **iii**) The ΔEPSPs (EPSP1 to EPSP3) measured on the individual trials tended to show more depression for a PF-CF pairing interval of 120 ms, than those measured during the no CF control trials (*open symbols*). **iv)** Averages across trials for the data shown in *iii*. **** $p < 0.00001$, t-test, mean ± S.E.M.

Fig. S2C. PF EPSPS were stable if not paired with a CF i) The change in parallel fiber-to-Purkinje cell EPSP amplitude (ΔEPSP) on each trial was measured in the flocculus, during the no-CF control condition (*red arrowhead* indicates omitted CF stimulus) used for the single-trial plasticity experiments *(top schematic)*, and there was no change over time. **ii)** Averaged over more than 10 min, the ΔEPSP was close to zero. **iii)** Associated changes in input resistance and access resistance for these cells (See Supplemental Experimental Procedures). n = number of cells, mean ± S.E.M.

Fig. S2D. CF alone (no PF) controls, in the flocculus. i) Schematic of experimental design. *Top:* In the no-PF control trials, the CF activation was delivered without paired PF activation (*arrowhead* indicates omitted PF stimulus). *Bottom:* In other trials, the CF was paired with the PF at a 120 ms delay. **ii)** A PF-CF interval of 120 ms induced single trial depression, as in the cells in Fig. 2B, which was significantly greater than that observed in the no-PF control condition, * $p < 0.05$, t-test, mean ± S.E.M.

Fig. S2E. PF-CF pairing does not induce a change in input or access resistance. i) Schematic of experimental design. The PF stimuli used to measure single-trial depression (EPSP1 and EPSP3) before and after a PF-CF pairing at 120 ms, were replaced by a hyperpolarizing current step, in order to assess changes in input and access resistance. **ii)** There was no change in input resistance (*black bar*, mean ± S.E.M., n = 10 cells) after PF-CF pairing at 120 ms. **iii)** There was no change in access resistance induced by PF-CF pairing at 120 ms. Bridge-balanced responses to hyperpolarizing current steps are shown for all 10 cells before (*black)* and after *(red)* PF-CF pairing, mean ± S.E.M.

Fig. S2F. Changes in membrane voltage do not underlie selective depression at a PF-CF interval of 120 ms in the flocculus. i) Example trace showing measurement of membrane potential (V_m) just prior to the measurements of the PF-to-PC EPSPs, before (EPSP1) and after (EPSP3) a PF-CF pairing. These measurements were used to calculate $\Delta V_m = V_m(\text{EPSP3}) - V_m(\text{EPSP1})$ for each trial in the single-trial plasticity experiments shown in Fig. 2B. **ii)** There was no difference in ΔV_m across the different PF-CF pairing intervals. For all cells shown in Fig. 2B, the mean ΔV_m was less than 0.5 mV, and was indistinguishable across different PF-CF intervals. Mean ± S.E.M.

Fig. S2G. Raw firing rates for *in vivo* trial-by-trial analysis. i) Mean Purkinje cell firing rates for cells used in Fig. 2C, aligned to trial start. **ii)** Baseline-subtracted Purkinje cell firing rates used for Fig. 2C. *Blue* = CF pairs: pairs of trials where there was a climbing fiber spike on the first trial and not on the second. *Black* = No-CF pairs, where there was no climbing fiber spike on either trial. Dotted lines show the mean for the first trials, and continuous lines show the mean for the second trials, aligned to the time of the climbing fiber spike (for more detail, including alignment of No-CF pairs, see Supplemental Experimental Procedures), mean ± S.E.M. The *in vivo* plasticity shown in Figure 2C could, in principle, reflect changes at the PF-to-PC synapses or any of several other synaptic sites (Mittmann and Häusser, 2007), but the similar timing for the single-trial plasticity at the PF-to-PC synapses (Figure 2B) makes it a candidate mechanism for the *in vivo* changes.

FIGURE S3

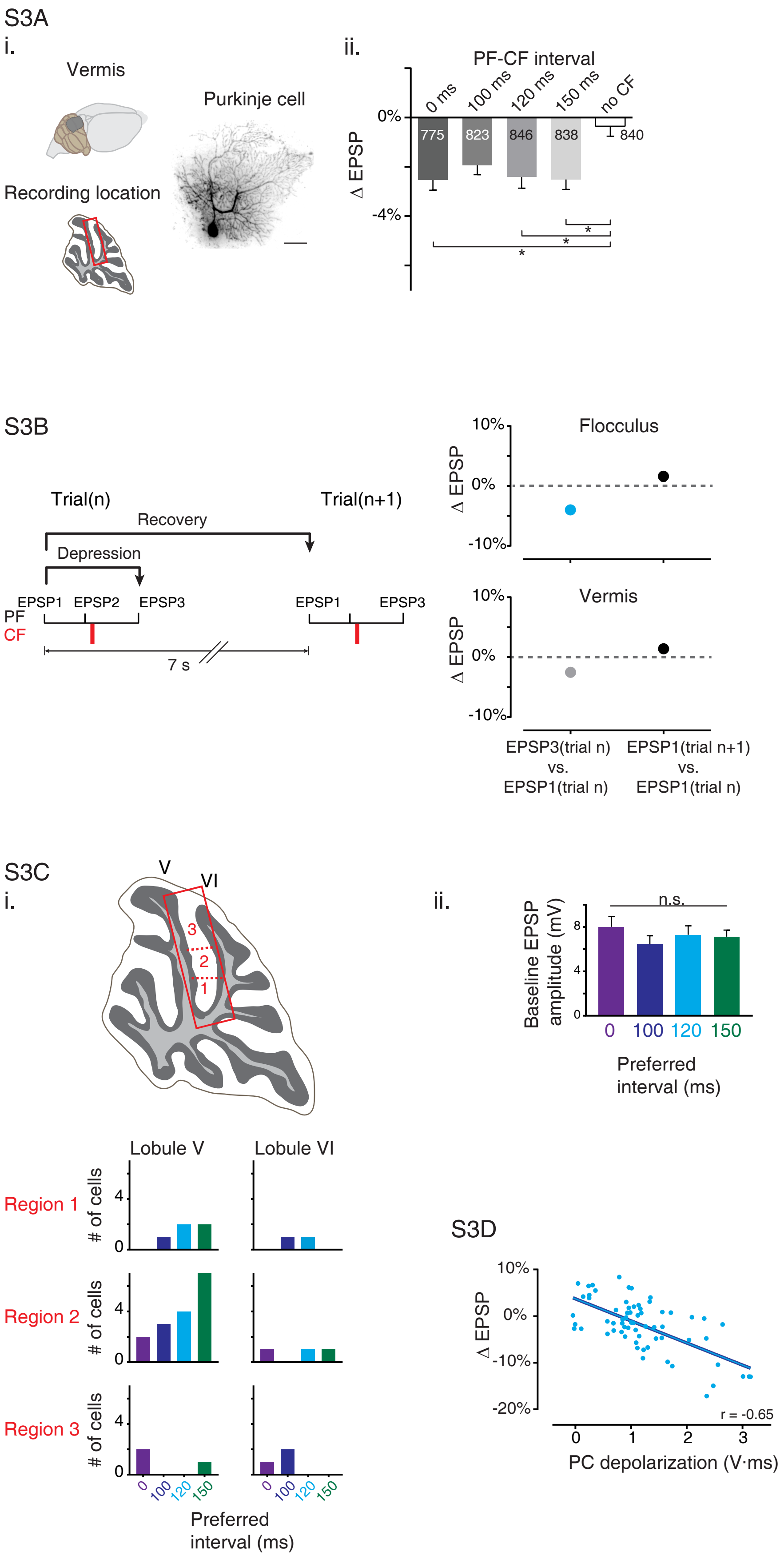
S3A
i.
Vermis
Purkinje cell
Recording location
ii.
PF-CF interval
0 ms
100 ms
120 ms
150 ms
no CF
0%
-4%
Δ EPSP
775
823
846
838
840
*
*
*
S3B
Trial(n)
Trial(n+1)
Recovery
Depression
EPSP1
EPSP2
EPSP3
EPSP1
EPSP3
PF
CF
7 s
Flocculus
Vermis
10%
0%
-10%
Δ EPSP
EPSP3(trial n) vs. EPSP1(trial n)
EPSP1(trial n+1) vs. EPSP1(trial n)
S3C
i.
V
VI
3
2
1
Lobule V
Lobule VI
Region 1
Region 2
Region 3
# of cells
Preferred interval (ms)
0
100
120
150
ii.
n.s.
Baseline EPSP amplitude (mV)
Preferred interval (ms)
S3D
Δ EPSP
10%
0%
-10%
-20%
r = -0.65
PC depolarization (V·ms)

Supplemental Figure 3 (Related to Figure 3)

Fig. S3A. Single-trial plasticity analyzed by averaging across trials rather than across cells confirms that depression was not tuned to a single PF-CF interval in the vermis. i) *Top left:* Lobules V-VI of vermis, shown in grey. *Bottom left:* Recording location illustrated in the parasagittal plane (*red box*). *Right:* Dye-filled Purkinje cell from the vermis, scale bar 20 µm. Maximum-intensity projection of Z-stacks. Gamma-filtering was used on each image of a Z-stack to compensate for differences in absolute intensity along the depth of the slice (see Supplemental Procedures). **ii)** Single-trial data from the vermis, shown in Fig. 3A, analyzed by pooling the 19-25 trials at each PF-CF interval for each cell, across all cells and averaging, instead of using a single average value for each PF-CF interval for each cell. * $p < 0.05$, one way ANOVA on ranks followed by Dunn's pairwise comparison, n = number of trials, shown inside bars, mean ± S.E.M.

Fig. S3B. Single-trial depression of PF-to-PC synapses recovers between trials. *Left:* Schematic illustrating the analysis for measuring single-trial synaptic depression, and recovery from one trial to the next. *Right:* A single PF-CF pairing at an interval of 120 ms in the flocculus (*top*) and 0 ms in the vermis (*bottom*) decreased the amplitude of the EPSP elicited in the Purkinje cells by PF stimulation after pairing, as compared with before pairing (EPSP3(trial n) vs. EPSP1(trial n); *grey or light blue;* re-plotted from Fig S2Aii and S3Aii). However, the EPSP amplitude recovered by the beginning of the next trial (*black*, EPSP1(trial n+1) vs. EPSP1(trial n)), which was 6 s after the PF-CF pairing, since the time from the start of one trial to the next was 7 s. n =774 trials from 470 trials from 19 cells in flocculus and 31 cells in vermis. Mean ± S.E.M., error bars smaller than symbol size.

Fig. S3C. PF-CF interval that induces maximum single-trial depression in the vermis was not related to spatial localization or EPSP amplitude. i) Cells shown in Fig. 3 were recorded from lobules V and VI of slices of the vermis. *Top cartoon* shows a parasagittal slice of vermis divided into three regions. *Below:* Number of cells recorded from each region, plotted according to preferred PF-CF interval: 0 ms *(purple)*, 100 ms *(dark blue)*, 120 ms *(light blue)* or 150 ms *(green*). There was no clear organization of cells that preferred different PF-CF intervals by region within lobules V and VI. **ii)** Baseline EPSP amplitude was not different between cells which preferred different PF-CF intervals (repeated measures ANOVA on ranks), mean ± S.E.M.

Fig. S3D. Single-trial plasticity was correlated with PC depolarization in the flocculus. For flocculus Purkinje cells shown in Fig. 2B, single-trial synaptic depression (ΔEPSP) in each cell, for each PF-CF interval, was correlated with the amount of Purkinje cell depolarization, as shown for vermis in Fig 3E (See Fig. 3C and Supplemental Experimental Procedures for how Purkinje cell depolarization was measured).

FIGURE S4

S4A

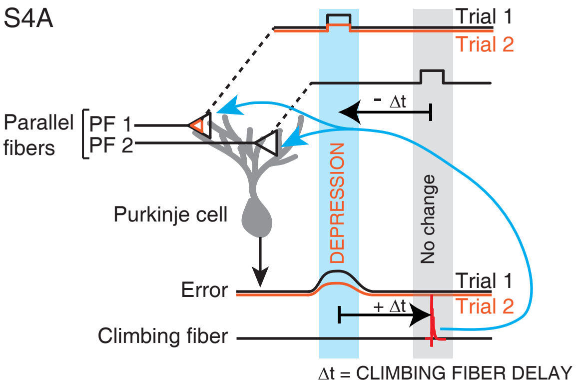

S4B

i.

ii.

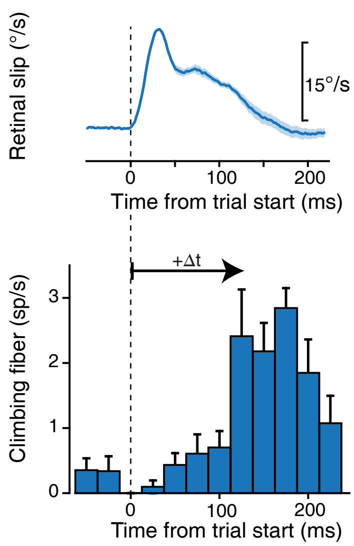

Supplementary Figure 4 (related to Fig. 4)

Fig. S4. Error signals carried by climbing fibers are delayed relative to motor performance errors.

A) The activity of some parallel fibers (PF1) contributes to a motor error on Trial 1. The error elicits a spike in the climbing fiber at a delay, Δt, relative to the activity of the parallel fibers that contributed to the error. Synapses that contributed to the motor error (PF1) are selectively depressed by the climbing fiber. Parallel fiber synapses active at the same time as the climbing fiber spike (PF2) did not contribute to the error, and are not depressed by the climbing fiber. Thus, climbing fiber-triggered plasticity compensates for the delay (Δt) in the error signals carried by the climbing fibers, by inducing depression of the parallel fiber synapses that were active at a time, $-\Delta t$, before the climbing fiber spike, providing a mechanism for solving the temporal credit assignment problem.

B i) During vestibulo-ocular reflex (VOR) learning (Fig.2C, D), image motion on the retina (retinal slip) indicates a performance error. VOR learning was induced by pairing a step of constant head velocity with motion of a visual stimulus (Kimpo et al., 2014; see Supplemental Experimental Procedures). Under such conditions, the eye movements fail to stabilize images on the retina, i.e., there is retinal slip, especially in the early part of the combined visual-vestibular stimulus, before visually-driven eye movements begin to compensate for an inadequate VOR.

ii) The retinal slip signaling an error is encoded by the climbing fibers, with firing delayed >100 ms (*arrow,* $+\Delta t$), relative to the onset of image motion ($t = 0$). Previous work has shown that when the timing of the error is precise, the timing of the climbing fiber response is also precise (Raymond and Lisberger, 1998), consistent with the more general role of the cerebellum in precise timing (Ivry and Spencer, 2004). In the specific VOR learning task used for the present analysis, the error is extended in time, and therefore the climbing fiber responses are also extended in time. We leveraged the trial-to-trial variation in the climbing fiber spike times to show that for each trial, the plasticity is precisely timed relative to each climbing fiber spike, rather than to some other task-related variable.

Supplemental Experimental Procedures

All protocols were approved by the Stanford Administrative Panel on Laboratory Animal Care.

In vitro slice electrophysiology.

Adult male C57Bl/6 mice (21-35 days) from Charles River Laboratories were used for all cerebellar slice recordings. Mice were kept on a 12 hour inverted day/night cycle and had *ad libitum* access to food and water. For cerebellar slice experiments, animals were anesthetized with isoflurane, cervically dislocated, and decapitated. The brain was extracted, and dissected under ice-cold artificial cerebrospinal fluid (aCSF (concentration in mM): NaCl(119), KCl(2.5), NaH_2PO_4(1), $NaHCO_3$(26.2), $MgCl_2$(1.3), $CaCl_2$(2.5), D-Glucose(10), equilibrated with Carbogen (95% O_2, 5% CO_2, Praxair)). 300 µm slices were made using a Leica VT1200 Vibrating Microtome. Because the cellular organization of the flocculus is rotated relative to the vermis (Fujita et al., 2012, 2014), the vermis was sliced parasagittally, and the flocculus coronally, in order to cut in a plane orthogonal to the parallel fibers, and parallel to the Purkinje cell dendrites (Fig. S2Ai, S3Ai). Slices were allowed to recover at 35°C for 30 min, and then at room temperature for 1 hour.

Slices were incubated in a recording chamber on an Olympus BX51WI upright microscope, in artificial cerebrospinal fluid maintained at 30-32°C. Purkinje cells were visualized with differential interference contrast optics, and recording was done in the whole-cell configuration. Stimulation was done using bipolar stimulating electrodes made from theta glass (Sutter Instruments), which were positioned in the outer third of the molecular layer in order to stimulate parallel fibers (PFs), and in the granule cell layer close to the Purkinje cell body in order to stimulate climbing fibers (CFs).

Patch electrodes (3-6 MOhms) were pulled from borosilicate glass tubing (Harvard Apparatus) and filled with an internal solution containing (concentration in mM): $KMeSO_4$(133), KCl(7.4), $MgCl_2$(0.3), HEPES(10), EGTA(0.1), MgATP(3), Na_2GTP(0.3), pH adjusted to 7.3 with KOH, osmolarity 260-290 mOsm. 100 µM picrotoxin was added to the aCSF to block $GABA_A$ channels. Cells were held in voltage clamp at -70 mV or in current clamp. Signals were acquired at 20 kHz using a Multiclamp 700B amplifier and low-pass filtered at 10 kHz. Access resistance was < 25 MOhms and both input and access resistance were monitored for stability throughout the recording.

All aCSF reagents and picrotoxin were obtained from Sigma-Aldrich, except NaCl (both from Sigma-Aldrich and from AMD chemicals) and KOH, which was obtained from AMD chemicals. Slice physiology data were analyzed in pCLAMP 10 (Clampfit) or MATLAB, with statistical tests performed using SigmaPlot or GraphPad Prism (see section on Statistics).

Long-term plasticity *in vitro*.

Long term plasticity at parallel fiber-to-Purkinje cell (PF-to-PC) synapses was induced by parallel fiber-climbing fiber (PF-CF) pairings repeated 300 times at 1 Hz, delivered ≤15 minutes after whole-cell recording began. Parallel fiber and climbing fiber stimuli were each 150 µs long. Each climbing fiber stimulus was paired with an individual parallel fiber stimulus, or a brief train of five parallel fiber stimuli at 100 Hz. These stimulation procedures are commonly used in studies of cerebellar LTD, and thus facilitate comparison with previous findings (Coesmans et al., 2004; Hansel and Linden, 2000; Wadiche and Jahr, 2005; Wang et al., 2000).

The interval between the parallel fiber and climbing fiber stimuli (PF-CF interval) varied across experiments (0, 100, 120 or 150 ms). When a parallel fiber train was paired with the climbing fiber, the PF-CF interval was measured from the middle of the parallel fiber train, except in one cell where it was measured from the second pulse in the train. Cells were held in current clamp during the induction of plasticity to permit climbing fiber-driven complex spikes (Hansel et al., 2006; Sarkisov and Wang, 2008).

Before and after pairing, the strength of PF-to-PC synapses was tested with parallel fiber stimulation at 0.05 Hz. In some experiments, cells were held in current clamp during testing; and in some experiments, the cells were held in voltage clamp (-70mV) during testing. In the long-term current clamp recordings, capacitance was compensated, bridge was balanced, and sufficient current (<1 nA) was injected for an initial baseline membrane voltage between -69 and -75 mV. In a subset of the voltage clamp recordings, series resistance was compensated. Series and input resistance were monitored, and changed by <20% throughout the recording. EPSP or EPSC amplitude was measured in Clampfit.

Measurements of input and access resistance (Supplemental Figures S1C; S2C) were obtained from the response to a hyperpolarizing current or voltage step delivered after every EPSP/EPSC measurement, measured in Clampfit. All EPSP and EPSC example traces shown in all figures were low-pass filtered at 500 Hz, and stimulus artifacts were truncated.

Single-trial plasticity *in vitro*.

Short-term plasticity induced by a single PF-CF pairing was characterized in slices from the flocculus and vermis. In these experiments, each trial consisted of a single pairing of parallel fiber and climbing fiber stimulation, plus two tests of the synaptic response to the parallel fiber stimulation alone. The parallel fiber stimulation that was paired with climbing fiber stimulation (Fig. 2A, PF EPSP2) was delivered at 0 ms (i.e. coincident with), 100 ms, 120 ms or 150 ms before climbing fiber stimulation. The test pulses were delivered to the parallel fibers 1 s before and 1 s after climbing fiber stimulation (Fig. 2A, PF EPSP1 and PF EPSP3), and these measurements were used to calculate the percent change in EPSP amplitude for that trial. For the analyses in Fig. 2B and 3A, B, the change in the EPSP measured on all trials of a given type (PF-CF pairing interval or control) in one cell were averaged, and then each cell contributed a single average value for the change in the EPSP. For Fig S2A and S3A, all trials across all cells, for a given PF-CF interval, were pooled and then averaged. Initial baseline membrane voltage was between -60 mV and -75 mV, as for LTD studies (Coesmans et al., 2004; Hansel et al., 2006) (<1nA injected).

Parallel fiber and climbing fiber stimulus pulses were 150 μs long. Parallel fibers were activated with one pulse. Climbing fibers were activated with two stimulus pulses, 10 ms apart. Two stimuli were delivered to climbing fibers in order to broaden the complex spike, because *in vivo,* single trial plasticity is observed only on trials when the width of the complex spike is broad (Yang and Lisberger, 2014). Climbing fibers are known to transmit brief, high-frequency bursts of ~10 ms in duration, and it has been shown that stimulation of the climbing fibers with a 10-ms train rather than a single pulse broadens the complex spike and increases the probability of LTD (Mathy et al., 2009; see also Rasmussen et al., 2013). Paired stimulation of parallel fibers and climbing fibers was done in current clamp to allow depolarization during the climbing fiber-triggered complex spike, which is necessary for induction of plasticity.

The same cells were tested with PF-CF pairing intervals of 0, 100, 120, and 150 ms, as well as with control trials in which the PF-CF pairing was replaced with a single stimulus to the PF alone or the CF alone. For the "No CF" control condition, three parallel fiber stimuli were given at the same time points as in the 120 ms PF-CF interval condition, but without the CF stimulation. Each cell underwent 19-25 trials at each PF-CF interval. Trials with the same PF-CF pairing interval were delivered in blocks of 10-25 trials, with trial start times 7 s apart. Blocks were presented in pseudorandom order.

We quantified the extent to which the Purkinje cell depolarized during the complex spike as the area under the curve (Fatt and Katz, 1951) of the Purkinje cell voltage during the complex spike (Fig. 3C), a measure similar to charge transfer measured in voltage clamp (Arenz et al., 2008). The area under the complex spike waveform was measured in a 150 ms window after the climbing fiber stimulus, relative to the baseline membrane potential immediately prior to PF-EPSP 2 (see Fig. 3C for schematic showing measurement area). If, during the 150 ms analysis window, there was post-complex spike hyperpolarization below the baseline, the area of the hyperpolarization was subtracted from the area of the depolarization.

The tuning of single trial plasticity for the PF-CF interval was quantified with a Selectivity Index (SI), calculated as SI = (Depression at preferred interval – Average depression at the three non-preferred intervals) ÷ Depression at preferred interval (Van Hooser, 2005). Cells that exhibited <1% depression at the preferred interval were excluded from the calculation of the selectivity index to avoid spuriously high selectivity indices (Mazurek et al., 2014). A selectivity index of zero indicates no difference in the amount of depression induced by the different PF-CF pairing intervals tested, i.e. equal depression at all intervals, whereas a selectivity index of 1.0 indicates depression at the preferred interval and no depression, on average, at non-preferred intervals. A selectivity index greater than 1.0 is also possible if there is potentiation, rather than depression, at the non-preferred intervals.

Statistics.

For all statistical analyses, a D'Agostino-Pearson test for normality was performed to determine whether a parametric or non-parametric test should be performed. For current- and voltage-clamp measurement of long-term plasticity (Fig. 1B, 1D), significance was assessed using a Mann-Whitney test. Long-term plasticity induced by different PF-CF intervals (Fig. 1C) was compared using a Kruskall-Wallis ANOVA on ranks, followed by a Dunn's pairwise comparison. Single-trial data from the flocculus (Fig. 2B) were analyzed using a repeated measures ANOVA on ranks, followed by a post-hoc Student-Neuman-Keuls pairwise comparison. Single-trial data from the vermis (Fig. 3A) were analyzed using a repeated measures ANOVA, followed by a post-hoc Student-Neuman-Keuls pairwise comparison. Selectivity index data in Fig. 3F were compared using a Mann-Whitney test. Single-trial data in Supplemental figures S2A, S3A were analyzed using a Kruskall-Wallis ANOVA on ranks followed by Dunn's pairwise comparison. Comparison of the no-CF vs. 120 ms PF-CF pairing trials for an example cell (Fig. S2B iv), and comparison of the summary data for CF-alone control trials vs. 120 ms PF-CF interval trials (Fig. S2D ii) were each done with a Student's t-test. Comparison of membrane potential across PF-CF intervals (Fig. S2F) was performed with a repeated measures ANOVA, and comparison of baseline EPSP amplitude across different cells in the vermis (Fig. S3C ii) was done with a Kruskall-Wallis ANOVA on ranks. Statistical tests were done in GraphPad Prism, except for ANOVAs with post-hoc measurements, which were done using SigmaPlot.

Single trial *in vivo* plasticity.

Previously published data (Kimpo et al., 2014) from two awake, behaving, male rhesus monkeys were reanalyzed to align trial-to-trial changes in Purkinje cell simple spike firing rates and eye movements to the time of the associated climbing fiber spike. Extracellular recordings were made of the simple spikes and complex spikes of isolated Purkinje cells during vestibulo-ocular reflex (VOR) gain-increase training, which paired vestibular stimuli (head turns) with image motion in the opposite direction. The vestibular stimuli (250 ms or 500 ms steps of head velocity at 15˚/s) were delivered by passive rotation of the animal about an earth-vertical axis. Visual stimuli consisted of a projected black-and-white pattern with a small central fixation target, and moved in the opposite direction from the vestibular stimulus at 15˚/s. Horizontal eye position (relative to the head) was measured using the eye coil method (Robinson, 1963), and was converted to eye velocity using a hardware differentiator and 300 Hz low-pass filter. Large saccades were identified using an automatic velocity threshold algorithm, and the corresponding eye velocity data excluded from the analysis. Remaining small saccades were removed manually. If more than 50 ms of a trial was marked by a saccade, the entire trial was excluded from the analysis.

Single units were recorded extracellularly in the flocculus and ventral paraflocculus using platinum-iridium electrodes. The cells included in the analysis were all identified as horizontal gaze velocity Purkinje cells (Raymond and Lisberger, 1998). Since spikes in a climbing fiber elicit a characteristic complex spike in their Purkinje cell targets in a one-to-one manner (Eccles et al., 1966), the complex spikes provide a readout of spikes in the climbing fiber input, hence we refer to a complex spike as a "climbing fiber spike." Simple spikes and complex spikes were identified as described previously (Kimpo et al., 2014) and Purkinje cell output firing rates were calculated using the reciprocal interval method (Lisberger and Pavelko, 1986). VOR learning trials were sorted according to whether or not there was a climbing fiber spike in the window 75-250 ms after onset of the visual-vestibular stimulus. Each pair of consecutive trials in which there was a climbing fiber spike on the first trial, but not on the second trial was classified as a CF trial pair. Each pair of consecutive trials in which there was no climbing fiber spike on either trial was classified as a No CF trial pair. The Purkinje cell firing in the first trial was then subtracted from that in the second trial to obtain the trial-to-trial changes in firing rate. The trial-to-trial changes in firing for each CF trial pair were aligned to the time of the climbing fiber spike and then averaged (Fig. 2C). The trial-to-trial changes in firing for the No CF trial pairs were aligned on randomly selected times of a climbing fiber spike from the CF trial pairs (both trials of a No CF pair aligned on the same time), so that the populations of CF and No CF trial pairs were aligned to the same distribution of climbing fiber spike times from within the 75-250 ms analysis window. Similarly, eye velocity during the first trial in a pair was subtracted from that in the second trial to obtain the trial-to-trial changes in behavior (Fig. 2D). Negative values (Fig. 2D) indicate eye movement in the direction opposite to head rotation, so that a more negative value represents an adaptive increase in VOR amplitude. Trial-to-trial changes in Purkinje cell firing rate and eye velocity were analyzed in MATLAB (Mathworks Inc.). Trial-to-trial changes were first averaged across trials within a cell, and Purkinje cell firing rates were smoothed with a 25 ms sliding average window. Finally, data were averaged across cells (n=9) for each condition.

Trial-to-trial changes were only analyzed for times preceding the climbing fiber spike by more than 10 ms, due to artifacts caused by smoothing of the typical post-complex spike pause in simple spike firing. Bootstrapping was used to assess significance of changes in Purkinje cell firing rates and eye velocity. For each cell, pairs of consecutive trials were randomly selected from the pool of all consecutive trials, to match the quantity of CF trial pairs that were included in the average for that cell. Average trial-to-trial changes were then calculated and averaged for each cell as described above, and a grand average for all cells was determined. This process was repeated 1000 times to create a bootstrapped distribution for both firing rate and eye velocity. Observed trial-to-trial changes in Purkinje cell firing rates and eye velocity were determined to be significant if they exceeded the 95% confidence intervals of each bootstrapped distribution (dashed lines in Fig 2C and D).

Estimation of climbing fiber delay in mice.

For the analysis in Supplemental Fig. S1A, climbing fiber responses during optokinetic reflex adaptation in mice (Goossens et al., 2004) were analyzed to estimated climbing fiber delays using the same method previously used to estimate the delays in the error signals carried by the climbing fibers during oculomotor learning in monkeys (Raymond and Lisberger, 1998). The phase of peak climbing fiber firing relative to the optokinetic stimulus was first calculated from the published mouse data (Goossens et al., 2004) by adding together complex spike phase relative to eye, with eye phase relative to the optokinetic stimulus. The phase of climbing fiber firing relative to the optokinetic stimulus exhibited a progressive lag with increase in stimulus frequency from 0.1 Hz to 0.8 Hz. This phase lag was fit with a fixed delay by fitting the equation: $\theta = R + 2\pi fT$, where θ is the phase of the climbing fiber firing relative to the visual stimulus, T is the predicted climbing fiber delay, f is the frequency of the training stimulus and R is a constant reference point on the visual stimulus. This yielded an estimate of 121 ms for the climbing fiber delay (T) in mouse Purkinje cells, a value similar to the 122 ms estimated in monkeys. Published data for a 0.05 Hz optokinetic stimulus were excluded from the analysis because of the extremely low amplitude of the climbing fiber response, which would make determination of the phase less certain, and because the measured phase of the climbing fiber firing during the 0.05 Hz optokinetic stimulus lagged rather than led the phase at 0.1 Hz, making it impossible to fit with a delay.

Purkinje cell dye fills.

100 mM Alexa Fluor-488 hydrazide sodium salt (Life Technologies) was added to the internal solution for dye-fill reconstructions of Purkinje cells. Whole-cell recording using the dye-containing internal solution was maintained for a minimum of 40 min, the pipette slowly retracted, and the slice fixed in 4% formaldehyde in 0.1X PBS. Cells were imaged using a Perkin-Elmer spinning-disk confocal microscopy system on a Zeiss Axioscope body, equipped with a 488 nm laser, a Hamamatsu EMCCD camera, and run by Volocity software. Gamma-filtering was used on each image of a Z-stack to compensate for differences in absolute intensity along the depth of the slice. Maximum-intensity projections of Z-stacks were then obtained using Fiji (ImageJ) software (Schindelin et al., 2012).

Antibody staining.

Brains from adult male C57 Bl6 mice (28-35 d old) were fixed in 4% formaldehyde in phosphate buffered saline (PBS) and then cryoprotected in buffered sucrose solution (30% in PBS). Immunohistochemistry was carried out on 20 micrometer thick coronal (for the flocculus) or sagittal (for the vermis) sections, made on a Leica CM3050 cryostat. Tissue sections were washed thoroughly in PBS containing 0.1% BSA, blocked in 10% Normal Goat Serum (NGS) containing 0.3% Triton X-100 for 1 hour at room temperature, washed in PBS with 0.1% BSA, and incubated in primary antibody overnight at 4˚C. Primary antibody was 1:5000 anti VGLUT1 Guinea pig polyclonal (Millipore AB5905), made in 2% NGS PBS with 0.1% BSA and 0.1% Triton X-100. Tissue sections were then washed, as previously, and incubated in secondary antibody for 1.5 hrs at room temperature. Secondary antibody was goat anti-guinea pig Secondary Antibody, Alexa Flour® 594 conjugate (Invitrogen A-11076) at 1:500 in 2% NGS in PBS with 0.1% Triton X-100. Sections were washed again, as previously, and mounted in Vectashield mounting medium containing DAPI. Images were acquired using a widefield fluorescence microscope system built around a Zeiss Axiovert 200M, equipped with a 100W HBO lamp and an ORCA Flash 4.0 LT sCMOS camera (Hamamatsu). A 10X, 0.3 NA objective was used and the system was controlled using µManager software (Edelstein et al., 2010).

Supplemental References

Arenz, A., Silver, R.A., Schaefer, A.T., and Margrie, T.W. (2008). The contribution of single synapses to sensory representation in vivo. Science (80-.). *321*, 977–980.

Chung, H.J., Steinberg, J.P., Huganir, R.L., and Linden, D.J. (2003). Requirement of AMPA receptor GluR2 phosphorylation for cerebellar long-term depression. Science *300*, 1751–1755.

Coesmans, M., Weber, J.T., De Zeeuw, C.I., and Hansel, C. (2004). Bidirectional parallel fiber plasticity in the cerebellum under climbing fiber control. Neuron *44*, 691–700.

Eccles, J.C., Llinas, R., and Sasaki, K. (1966). The excitatory synaptic action of climbing fibres on the Purkinje cells of the cerebellum. J. Physiol. 268–296.

Edelstein, A., Amodaj, N., Hoover, K., Vale, R., and Stuurman, N. (2010). Computer control of microscopes using manager. Curr. Protoc. Mol. Biol. 1–17.

Fatt, P., and Katz, B. (1951). An analysis of the end-plate potential recorded with an intra-cellular electrode. J. Physiol. *115*, 320–370.

Fujita, H., Morita, N., Furuichi, T., and Sugihara, I. (2012). Clustered fine compartmentalization of the mouse embryonic cerebellar cortex and its rearrangement into the postnatal striped configuration. J. Neurosci. *32*, 15688–15703.

Fujita, H., Aoki, H., Ajioka, I., Yamazaki, M., Abe, M., Oh-Nishi, A., Sakimura, K., and Sugihara, I. (2014). Detailed expression pattern of aldolase C (aldoc) in the cerebellum, retina and other areas of the CNS studied in aldoc-venus knock-in mice. PLoS One *9*, e86679.

Goossens, H.H.L.M., Alphen, A.M. Van, Steen, J. Van Der, Stahl, J.S., Zeeuw, C.I. De, and Frens, M.A. (2004). Simple spike and complex spike activity of floccular Purkinje cells during the optokinetic reflex in mice lacking cerebellar long-term depression. Neuroscience *19*, 687–697.

Hansel, C., and Linden, D.J. (2000). Long-Term Depression of the cerebellar climbing fiber–Purkinje neuron synapse. Neuron *26*, 473–482.

Van Hooser, S.D. (2005). Orientation Selectivity without Orientation Maps in Visual Cortex of a Highly Visual Mammal. J. Neurosci. *25*, 19–28.

Ivry, R.B., and Spencer, R.M.C. (2004). The neural representation of time. Curr. Opin. Neurobiol. *14*, 225–232.

Linden, D.J. (2012). A late phase of LTD in cultured cerebellar Purkinje cells requires persistent dynamin-mediated endocytosis. J. Neurophysiol. *107*, 448–454.

Lisberger, S.G., and Pavelko, T.A. (1986). Vestibular signals carried by pathways subserving plasticity of the vestibulo-ocular reflex in monkeys. J. Neurosci. *6*, 346–354.

Mazurek, M., Kager, M., and Van Hooser, S.D. (2014). Robust quantification of orientation selectivity and direction selectivity. Front. Neural Circuits *8*, 1–17.

Mittmann, W., and Häusser, M. (2007). Linking synaptic plasticity and spike output at excitatory and inhibitory synapses onto cerebellar Purkinje cells. J. Neurosci. *27*, 5559–5570.

Rasmussen, A., Jirenhed, D.-A., Zucca, R., Johansson, F., Svensson, P., and Hesslow, G. (2013). Number of spikes in climbing fibers determines the direction of cerebellar learning. J. Neurosci. *33*, 13436–13440.

Robinson, D.A. (1963). A method of measuring eye movement using a scleral search coil in a magnetic field. Bio-Medical Electron. IEEE Trans. *10*, 137–145.

Sarkisov, D. V, and Wang, S.S.-H. (2008). Order-dependent coincidence detection in cerebellar Purkinje neurons at the inositol trisphosphate receptor. J. Neurosci. *28*, 133–142.

Schindelin, J., Arganda-Carreras, I., Frise, E., Kaynig, V., Longair, M., Pietzsch, T., Preibisch, S., Rueden, C., Saalfeld, S., Schmid, B., et al. (2012). Fiji: an open-source platform for biological-image analysis. Nat. Methods *9*, 676–682.